Int J Adv Manuf Technol (2014) 72:1415–1427
DOI 10.1007/s00170-014-5744-4

ORIGINAL ARTICLE

Thermal error modeling of the spindle based on multiple variables for the precision machine tool

Yang Li · Wanhua Zhao · Wenwu Wu · Bingheng Lu · Yubao Chen

Received: 15 September 2013 / Accepted: 25 February 2014 / Published online: 20 March 2014

Abstract Thermal error, especially the one caused by the thermal expansion of spindle in axial direction, seriously impacts the accuracy of the precision machine tool. Thermal error compensation based on the thermal error model with high accuracy and robustness is an effective and economic way to reduce the impact and enhance the accuracy. Generally, thermal error models are built only on temperatures at some points in the spindle system. However, the thermal error is also closely related to other working parameters. Through the theoretical analysis, the simulation, and the experimental testing in this paper, it is found out that thermal error is determined by multiple variables, such as the temperature, the spindle rotation speed, the historical spindle temperature, the historical thermal error, and the time lag between the present and previous times. In order to examine the performance of thermal error models based on multiple variables, two common methods are used for modeling—the multiple regression method and the back propagation network. The data for modeling are collected from experiments conducted on the spindle of a precision machine tool under various working conditions. The modeling results demonstrate that models established based on the multiple variables have better accuracy and robustness. It also turns out that data filtering before modeling can further improve the performance of the models. Therefore, models based on multiple variables with good accuracy and robustness can be very useful for the further thermal error compensation. In addition, by taking relative importance analysis of multiple variables based on standardized regression coefficients, the influence of each variable to the thermal error is revealed. The ranking of coefficients can also be used as a new criterion for the optimal temperature variable selection in the future research.

Keywords Spindle thermal error modeling · Multiple variables · Multiple regression model · Back propagation network model · Standardized regression coefficients

Y. Li · W. Zhao · W. Wu · B. Lu
State Key Laboratory for Manufacturing System Engineering, Xi'an Jiaotong University, Xi'an, Shaanxi 710054, China

Y. Li
e-mail: 289163861@qq.com

Y. Chen
Department of Industrial and Manufacturing Systems Engineering, University of Michigan–Dearborn, Dearborn, MI 48128-1491, USA

W. Zhao (✉)
School of Mechanical Engineering, Xi'an Jiaotong University, No. 28 Xianning Road, Beilin District, Xi'an, Shaanxi Province 710049, China
e-mail: whzhao@mail.xjtu.edu.cn

1 Introduction

Among the errors detrimental to the precision of the machine tool, thermal error contributes significantly [1–3]. According to the research conducted by Professor Peklenik, the thermal error caused by the thermal deformation of machine tool counts for 40 to 70 % of the total manufacturing inaccuracy [4]. Compared with the ball screw, guide ways, and external thermal influences, such as the solar radiation and the ambient temperature, the spindle is the main thermal source of the machine tool. The spindle thermal error, especially the axial thermal error, has a great impact to the final machining accuracy [5–8].

In order to reduce the spindle thermal error, many methods have been developed. For example, some proposed design approaches, such as employing cooling system, heat pipes, thermally insensitive materials, and heat symmetrical structure, are used to minimize the thermal deformation [9, 10]. They either improve the heat dispelling or equalize the temperature field. However, these methods are uneconomic and have limited effectiveness in reducing the thermal error.

Because on the one hand, thermally insensitive materials, advanced cooling system, and heat pipes are expensive. On the other hand, the thermal error depends on the working conditions which are not usually under the designer's control [11, 12]. By contrast, another method called the thermal error compensation is more economical and efficient, as its principle is simple and can be easily realized in the factory with minimal cost. Thermal error compensation could be implemented by using the CNC controller to adjust and control the position of the tool. The position of the tool is dependent both on the demand of processing requirements and the thermal deformation of the spindle which can be predicted by the thermal error model. Therefore, establishing a thermal error model with high accuracy and robustness is the core of the thermal error compensation and the accuracy improvement. In general, the modeling methods include conventional linear regression [13], multiple regression[14], support vector machine [15], gray theory [16], Neural Network [17–19], etc. Most of existing models are built only on the temperatures of some points on the machine tool. In fact, the thermal deformation of the spindle depends on multiple variables (e.g., spindle rotation speed) and varies dramatically when the working condition changes [20].

In Section 2, factors related to the axial thermal deformation of the spindle are discussed based on the theoretical analysis, the finite element analysis (FEA), and experimental experiments. The results demonstrate that the thermal error of the spindle is determined by multiple variables. In Section 3, a series of tests conducted on a precision horizontal machining center are presented. The temperature sensors and Renishaw non-contact tool setting system NC 4 are used for measuring the temperature and the axial thermal deformation of the spindle under different working conditions, respectively. In Section 4, two common methods called multiple regression (MR) and back propagation (BP) network are applied to develop thermal error models. In these models, not only the temperature but also the speed, the historical temperature, the historical thermal error of the spindle, and the time lag between the present and previous times obtained from tests are used as the input data. The output data is the axial spindle thermal error which is more severe than the radial one [21]. The curve-fitting and predicted performances of the models demonstrate that models based on multiple variables have better accuracy and robustness. In addition, it was found that the data filtering can further improve the modeling performance. Finally, the relative importance of different variables is analyzed according to the standardized regression coefficients. The ranking of coefficients reveals that the historical temperature is critical to the thermal error modeling. It can also be used as a new criterion for the optimal temperature variable selection in the future research.

2 Analysis of the factors related to the spindle thermal error

2.1 Heat source and dissipation, temperature field, and thermal deformation

2.1.1 Heat source

In the spindle system, bearings are the main heat sources. The heat generation rate is Φ (W/m^2) which can be computed as follows [22, 23]:

$$\Phi = \frac{4iH_f}{L_{\text{sum}}\pi\left(d_1{}^2 - d_2{}^2\right)} \tag{1}$$

where H_f is the heat output of bearings (W); i is the number of bearings; d_1 and d_2 are the diameters of bearing outer ring and inner ring (m), respectively; L_{sum} is the sum of width of all the bearings and sleeve (m); n is the speed of the spindle (rpm).

$$H_f = 1.047 \times 10^{-4} nM \tag{2}$$

where M is the friction torque of bearings (N•mm) which can be computed according to functions 3 and 4 as follows:

$$M = M_1 + M_2 \tag{3}$$

$$M_1 = f_1 \cdot F_\beta \cdot d_m \tag{4}$$

$$M_2 = \begin{cases} 10^{-7} f_0 (vn)^{\frac{2}{3}} d_m{}^3 & vn \geq 2,000 \\ 160 \times 10^{-7} f_0 d_m{}^3 & vn < 2,000 \end{cases} \tag{5}$$

where f_0 and f_1 are the parameters related to the type, the structure, the force, and the lubrication of bearings; F_β (N) is the load determined by the magnitude and the direction of the force working on the bearings; v (cSt) is the kinematic viscosity of lubricant; d_m (m) is the diameter of the pitch circle.

From above Equations 1 to 5, it can be seen that the heat generation in spindle system is directly affected by the spindle rotation speed. For a certain spindle system under certain preload, the type, the structure, the size, and the lubrication of the bearings are known and regarded as unchanged. Then, it is obvious that the heat generation is increased with the increase of the spindle speed.

2.1.2 Heat dissipation

The convection of the cooling system is the major way of heat dissipation here because the precision machine tool is usually placed at a constant temperature workshop where the radiation and environmental variations are too small to be considered. The heat flow by convection H_v (W) can be calculated as follows:

$$H_v = h_v S(T_1 - T_2) \tag{6}$$

where h_v is the coefficient of convective heat transfer (W/(m^2•K)); S is the area perpendicular to the direction of the heat flux (m^2); T_1 and T_2 are the temperatures at two different moments (°C).

$$h_v = \frac{Nu \cdot \lambda}{l_e} \tag{7}$$

$$\begin{cases} Nu = 0.133 \mathrm{Re}^{\frac{2}{3}} \mathrm{Pr}^{\frac{1}{3}} \\ \mathrm{Re} = \dfrac{v_e l_e}{v} \\ l_e = \dfrac{\sum_i^n (d_i \cdot l_i)}{\sum_n l_i} \\ v_e = \dfrac{\pi l_e}{60} \cdot n \end{cases} \tag{8}$$

where Nu, Re, and Pr are the Nusselt number, the Reynolds number, and the Planck number, respectively. λ is the thermal conductivity (W/(m•K)); d_i and l_i are the diameter and the length of the ith part of the shaft (m), respectively.

From Equations 6 and 8 [22], it is known that together with temperatures, the rotation speed has a direct influence on h_v and further on the heat dissipation. Besides, in the transient state, the heat dissipation is unstable although under a certain running spindle speed as the temperatures are changing with the time. Therefore, the heat dissipation is also affected by the historical temperature data.

2.1.3 Temperature field

The temperature field of the spindle is dependent on the heat generation, the heat conduction, and the heat dissipation between different parts. The heat transfer in the spindle system is showed in Fig. 1.

To keep it simple, the spindle is regarded as one-dimensional rod with one end fixed. Based on the energy conservation law, the temperature can be computed as [24]

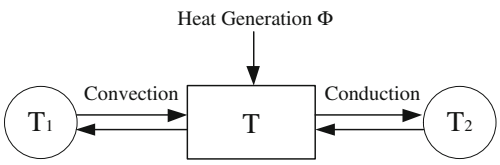

Fig. 1 Heat transfer in the spindle system

$$\sum H = H_{\mathrm{f}} + H_v + H_c = c_t \cdot \frac{dT}{dt} \tag{9}$$

where c_t is the heat capacitance (1/K).

The conduction heat (H_c) through a cross section of continuous material is [22]

$$H_{\mathrm{c}} = \lambda S \frac{dT}{dx} \tag{10}$$

According to Equation 9 and the discussion above, the temperature at one certain moment (T_i) is related to the Φ, H_v, H_c, and T_{i-1}(dT=T_i−T_{i-1}), which means that it varies with the spindle speed and historical data (the historical spindle temperature, the previous rotation speed, and the time lag between the present and previous times).

2.1.4 Thermal deformation

As the spindle is fixed at one end, the thermal deformation ΔL is

$$\begin{cases} \Delta \mathrm{L} = \alpha L (T_i - T_{i-1}) + \dfrac{\sigma L}{E} \\ \Delta \mathrm{L} = \dfrac{-P}{j} \\ P = A\sigma \end{cases} \tag{11}$$

$$\Delta \mathrm{L} = \frac{\alpha L A (T_i - T_{i-1})}{\frac{L}{Ej} + \frac{A}{j^2}} \tag{12}$$

where L and $\triangle L$ are the original length (m) and thermal deformation (m), respectively; T_i and T_{i-1} are the temperatures at t_i moment and t_{i-1} moment (°C); α is the thermal expansion

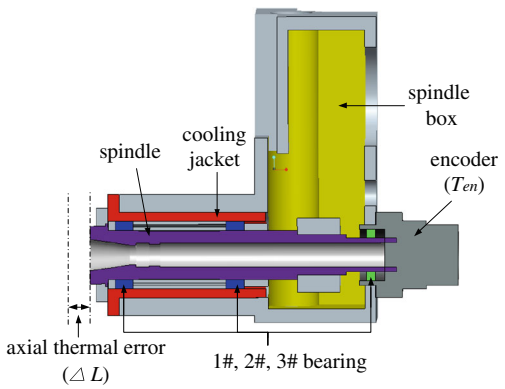

Fig. 2 Simplified geometrical model of the spindle system

Table 1 Simulation results of the temperature and thermal error of the spindle

T_{en} (°C)	$\triangle L$ (μm)	Spindle speed (rpm)	Historical running condition
26	40	4,000	Rotating, temperature is rising
	12	0	Resting, temperature is falling
30	55	4,000	Rotating , temperature is rising
	27	0	Resting, temperature is falling
35	72	4,000	Rotating , temperature is rising
	54	0	Resting, temperature is falling

coefficient (K^{-1}); σ, P, E, j, and A are the stress (MPa), the axial force (N), modulus of elasticity, the axial stiffness (N/m), and the area of the cross section (m^2), respectively.

From Equation 12, it can be seen that the thermal deformation of the spindle is dependent on T_i and T_{i-1} (α, P, E, j, and A are considered as constant) which are related to the spindle speed and historical running conditions.

In a word, according to the theoretical discussion above, thermal error is determined by multiple variables.

2.2 Finite element simulation

The structure of the spindle is showed in Fig. 2. Assuming that the spindle rotates at speed of 4,000 rpm for 3 h and then stops for 2 h, the heat loads and the convective heat transfer coefficient of different parts in the spindle system are computed and are then sent to the ANSYS/WORKBENCH for the finite element simulation.

Table 1 shows the simulated temperature of the encoder (T_{en}) and the axial thermal error of the spindle ($\triangle L$). After rotating for a while, the temperature of the encoder rises dramatically. This is because that the encoder is close to the heat source (3# bearing) and there is no cooling system at the end of the spindle system. It can be seen from Table 1 that when the temperature rises to 30 °C after spindle runs at 4,000 rpm for a moment, the thermal error reaches to 55 μm. When the temperature falls back to the same temperature (30 °C) after the spindle stops, however, the thermal error is 27 μm. It demonstrates that although the temperatures at a certain place are the same, the axial thermal error is different if the working conditions changed. It can also be concluded from finite element simulation results that the thermal error of the spindle is not only determined by temperature.

2.3 Experimental example

In order to verify that the thermal error depends on multiple variables in practical, three simple experiments are conducted on the spindle of a high-precision horizontal machining center. In tests 1 and 2, the spindle is rotating continuously at 3,000 and 4,000 rpm, respectively, until it reaches the thermal equilibrium. In test 3, the spindle speeds up from 0 to 5,000 rpm and then speeds down to 0 rpm. Figure 3 shows the relationship between temperature rise of the encoder and the axial thermal error of the spindle obtained from these three experiments. The setup of the experiments is introduced in Section 3.

From Fig. 3a, it can be seen that when the temperature is about 35 °C, the thermal error is 31.5 and 16 μm at the spindle speeds of 3,000 and 4,000 rpm, respectively. According to Fig. 3b, at the period of accelerating, the axial thermal error is 42 μm when the temperature rises to 40 °C. While, when the temperature falls back to 40 °C again at the period of speeding down, the thermal error changes to 63 μm. The reason why the thermal errors are different when the temperatures are the

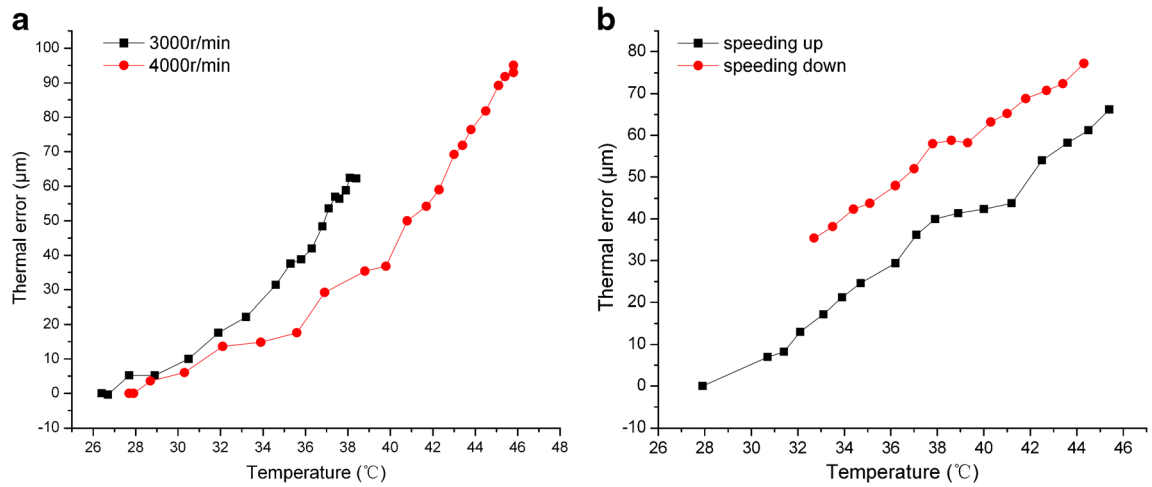

Fig. 3 The axial thermal error of spindle under different working conditions. **a** Tests 1 and 2, **b** test 3

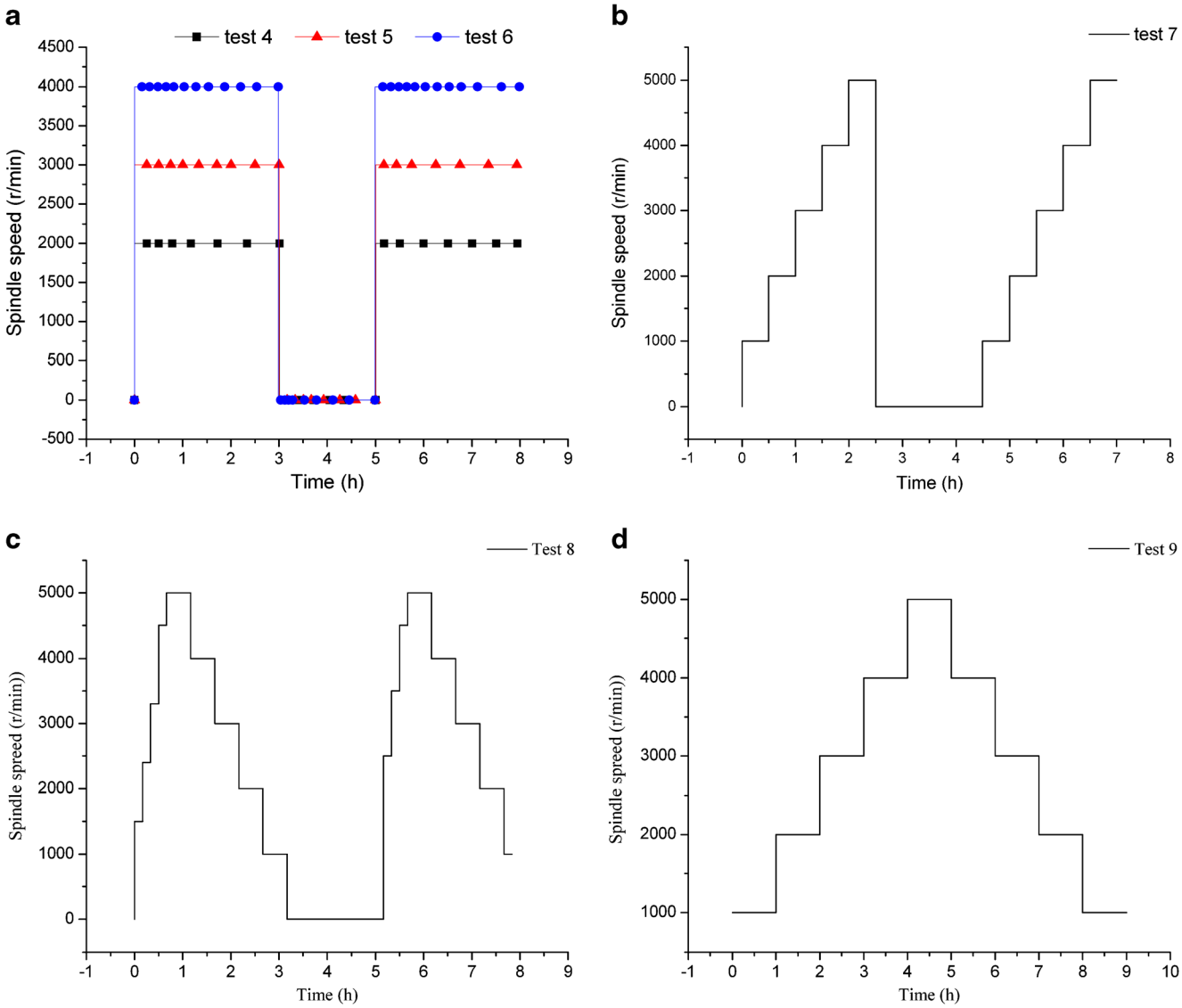

Fig. 4 Different working conditions. **a** Tests 4–6, **b** test 7, **c** test 8, **d** test 9

same is that the spindle speed has changed and the historical working conditions are different.

Based on the theoretical analysis, the simulation, and experimental results, it turns out that temperature is not the only factor impacting the thermal error. Therefore, it is necessary to consider multiple variables such as the working speed as well as the historical running conditions when trying to determine the thermal error of the spindle. Whether taking multiple

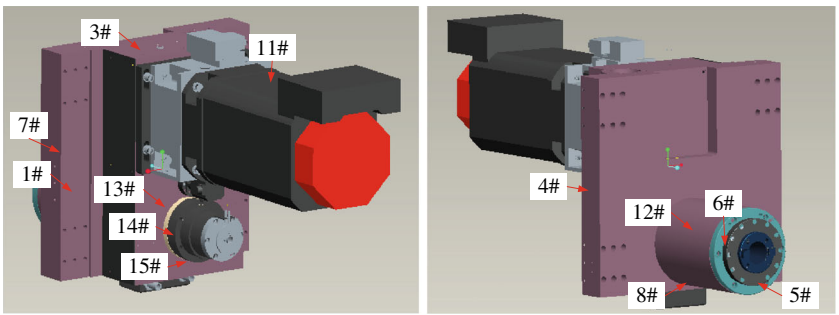

Fig. 5 Spindle temperature tests setup

variables as inputs for thermal error modeling can improve the accuracy and the robustness of modeling is discussed in Section 4.

3 Experimental tests

3.1 Test setup

Besides the three experiments in Section 2.3, other six different kinds of tests have been conducted. The nine experiments are renamed as tests 1–9. In these experiments, working conditions are considered as much as possible (Fig. 4). These working conditions include rotating in a constant speed, speeding up, speeding down, and running discontinuously, and so on.

In tests 1–3, the spindle is rotating at 2,000, 3,000, and 4,000 rpm continuously until the measured temperatures reach to a steady state. In tests 4–6, the spindle operates at a certain speed for 3 h, then stops for 2 h, and finally spins at the same speed for another 3 h. In test 7, the spindle is speeding up (0–5,000 rpm) in the first 2.5 h. After stopping for 2 h, the spindle runs from 0 to 5,000 rpm for another 2.5 h. In test 8, the spindle is required to speed down from 5,000 to 0 rpm and rest for 2 h in the middle. For security reasons, it takes about 0.8 h to speed up from 0 to 5,000 rpm rather than working at 5,000 rpm from the very beginning. In test 9, the spindle undergoes the acceleration stage first and then the deceleration stage. These tests with a pause in the middle simulate the daily working process in the factory, as operators always have a break at noon.

In these experiments, temperature sensors and Renishaw non-contact tool setting system NC 4 are used to test temperatures and axial thermal errors of the spindle [25]. Temperature sensors are placed at those places which are close to the heat source (bearings), and the sensors are distributed uniformly on the whole spindle system (Fig. 5 and Table 2). 2# temperature sensor is used to measure the ambient temperature in the working shop. 9# and 10# are placed at the nozzles

Table 2 Locations of the temperature sensors

Number	Location
3#	Top of the spindle box
4#, 7#	Two sides of the spindle box
1#, 13#	Back of the spindle box
14#, 15#	Encoder
8#, 12#	Spindle nose
5#, 6#	Spindle end
11#	Motor
9#, 10#	The nozzles of oil outlet pipes

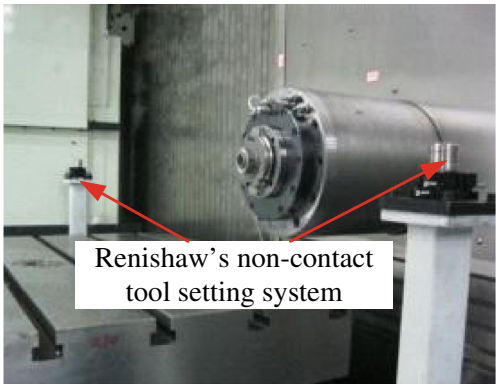

Fig. 6 Spindle axial thermal error tests setup

of two oil outlet pipes to test the oil temperature. Considering the temperature differences around the circumference at the spindle nose and spindle end, the angles between 8# and 12#, 5# and 6# are set as 90°. NC 4 (Fig. 6) is a tool providing high-speed/high-precision measurement of cutting tools on a machining center. It could be applied for testing the spindle axial thermal error.

3.2 Results of experiments

Figure 7 shows the experimental results of tests 1–3. The temperature and the thermal error rise with the increasing of the spindle speed. This is because that there is more heat generation at higher speed. When the spindle rotates at 4,000 rpm and reaches to the thermal equilibrium, the temperature is about 46 °C and the thermal error is 95 μm. By comparison, the temperature is only 32.5 and 38 °C, and the thermal error is 35.6 and 62.4 μm when the spindle runs at 2,000 and 3,000 rpm, respectively.

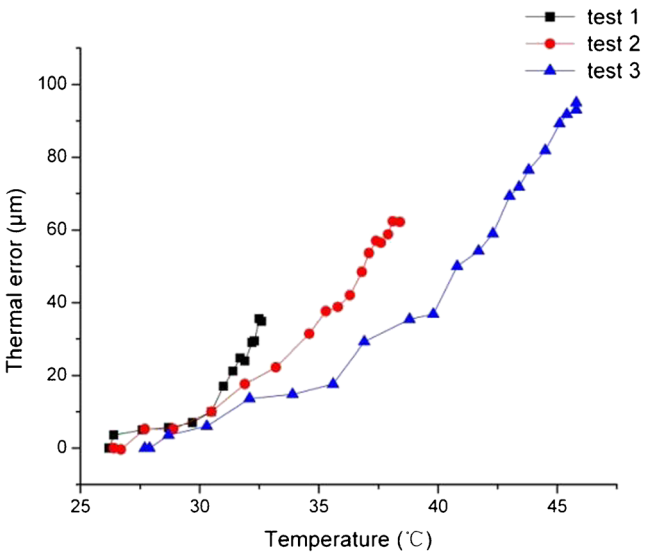

Fig. 7 Results of tests 1–3

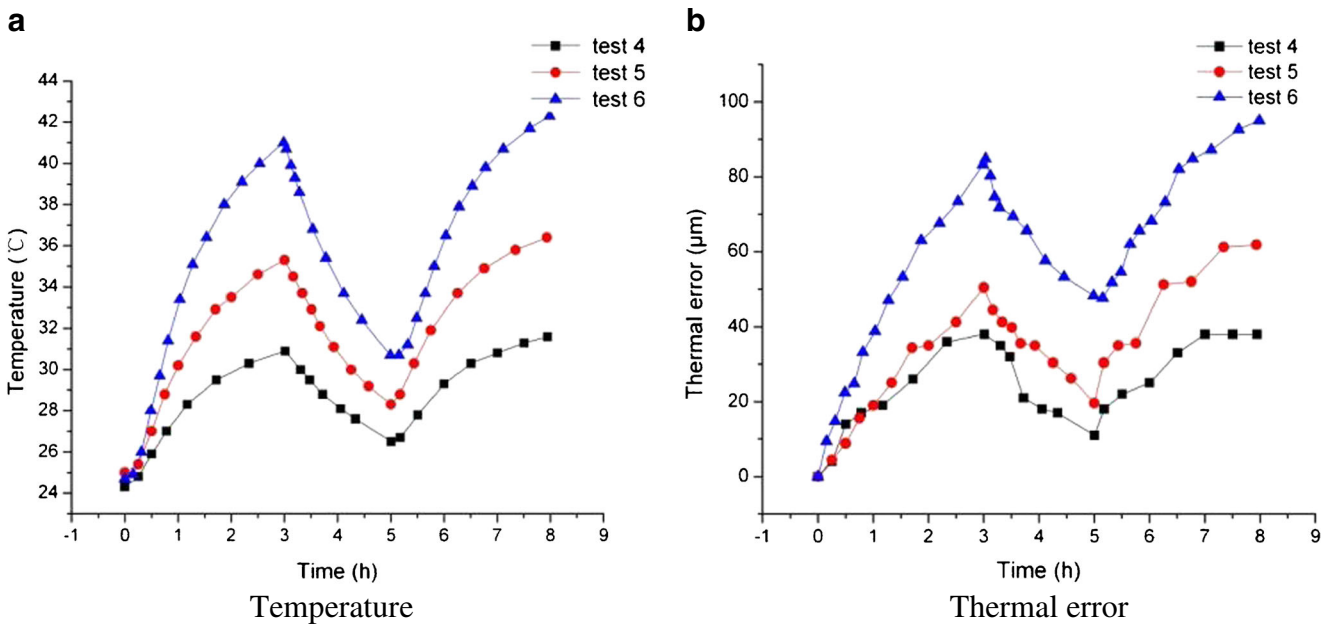

Fig. 8 Results of tests 4–6. **a** Temperature, **b** thermal error

According to the results of tests 4–6 (Fig. 8), the test process can be divided into three different stages. In the first stage, the spindle is rotating at 2,000, 3,000, and 4,000 rpm for 3 h, and the temperature and thermal error are increasing quickly. The temperature of the encoder reaches to 30.9, 35.3, and 41 °C while the thermal error is 38, 50.4, and 84.8 μm. In the second stage, the spindle stops for 2 h. The temperature and thermal error begin decreasing quickly, as there is only heat dissipation but no heat generation. Within 2 h, the temperatures drop about 4.4, 7, and 10.3 °C in tests 4, 5, and 6, while the thermal errors drop 27, 30.8, and 37.2 μm, respectively. The reason that the temperature and the thermal error change more considerably in test 6 than tests 4 and 5 is that the temperature is the highest in test 6 at the end of the first stage which leads to the most intense heat convection between spindle system and surroundings. In the third stage, the spindle rotates at the same speed as the one in the first stage for another 3 h. However, at the end of 3-h operating, the temperature of the encoder changes to 31.6, 36.4, and 42.3 °C, and the thermal error is 38, 62, and 95 μm at 2,000, 3,000, and 4,000 rpm. The temperatures and the thermal error obtained at the end of the first stage and the third stage are totally different although the spindle is running at the same speed for the same period of time. This is because that the initial condition of

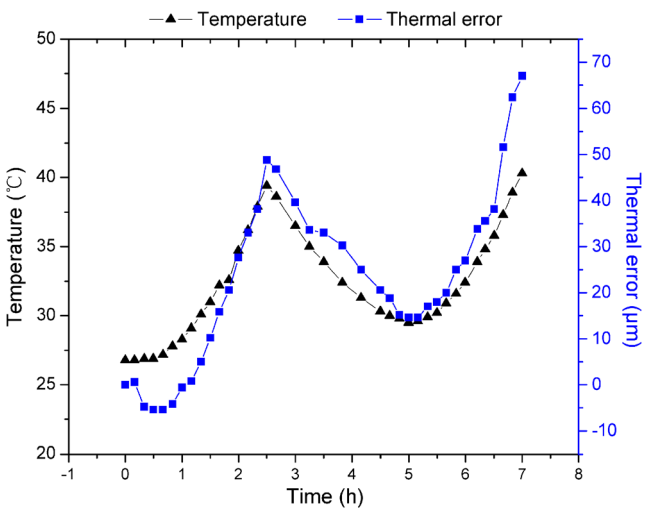

Fig. 9 Results of test 7

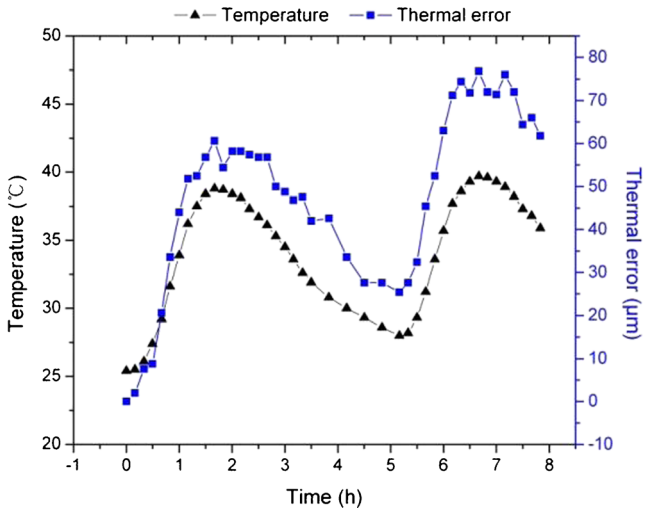

Fig. 10 Results of test 8

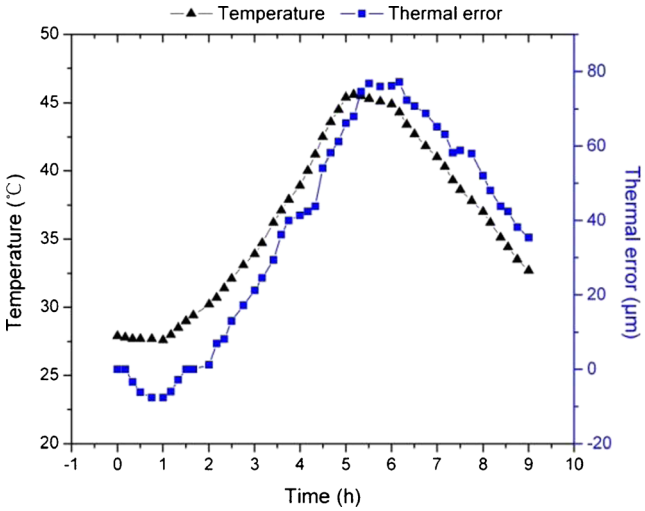

Fig. 11 Results of test 9

working has been changed. At the beginning of the first stage, there is no temperature rising and no thermal error. However, the initial temperatures in the third stage are 26.5, 32.1, and 40.7 °C at 2,000, 3,000, and 4,000 rpm and the axial thermal expansions are 18, 35, and 80.2 μm, respectively.

In test 7 (Fig. 9), the spindle speeds up from 0 to 5,000 rpm. The temperature of the encoder and the axial thermal error reaches to 39.4 °C and 48.8 μm after the first 2.5 h of working.

Also, the temperatures and the thermal error are higher than the ones in test 4 (30.9 °C, 38 μm) but lower than the ones in test 6 (41 °C, 83.2 μm). It may because that the heat generations are more but less in test 7 when accelerating than running at 2,000 and 4,000 rpm all the time. It means that the spindle speed plays a very important role in temperature and thermal error analysis. After 2 h of resting and another 2.5 h of running, the temperature and the thermal error changes to 40.3 °C and 67 μm, respectively. It is clear that from 0 to 2.5 h and from 4.5 to 7 h, the working conditions of the spindle are the same. However, the temperatures and thermal error at the end of these two processes are different. It is because that the historical conditions of them are different.

In test 8 (Fig. 10), the spindle experiences two deceleration stages (from 5,000 to 0 rpm) and stops for 2 h between these two stages. The temperature and the thermal error rise dramatically at first (0.5 to 1 h) as the high spindle speed (5,000 rpm) brings about large amount of heat. From 1.5 to 2 h, the spindle runs at 4,000 rpm, and the temperature and thermal error rise continuously when they first reach to the first peak at about 1.7 h—the temperature is 38.8 °C and thermal error is 60.6 μm. Then, the temperature and thermal errors fall down due to less heat generations at lower speed. At 5 h, the temperature and thermal error drop to 28 °C and 25.4 μm, respectively. The working condition from 5 to 7.5 h is the same with the one from 0 to 2.5 h. The encoder's temperature and the thermal error reach 39.7 °C and 76.8 μm, respectively, at the second peak (6.5 h). The temperature and the thermal error at 1 and 6 h are different although the spindle goes through the same acceleration process. This is because the historical data are not the same.

Figure 11 shows the results of test 9. It can be seen that the temperature and the thermal error reach to the peaks (45.6 °C and 68 μm) after 5 h of acceleration. Then, the values of temperature and the thermal error fall to 32.7 °C and 35.4 μm as the speed drops from 5,000 to 0 rpm. The curves of the temperature and the thermal error are asymmetric. When the temperature is 40 °C in the acceleration part, the thermal error is 42.4 μm. By comparison, when the temperature is 40 °C in the deceleration part, the thermal error turns to 63 μm. The difference is caused by the change of spindle speed and historical data.

All the tests results are used to verify that the thermal error is determined by multiple variables rather than the temperature

Fig. 12 Confidence intervals on the residuals

only. The results also provide enough data for optimal thermal error modeling in Section 4.

4 Thermal error modeling and optimization

In this section, two common methods, MR and BP, are applied to build thermal error models (see Sections 4.1 and 4.2). The modeling results are used to verify the correctness and the effectiveness of modeling based on multiple variables. Temperatures, the rotating speed, the thermal error at the present and the previous moments, and the time differences are taken as the input variables. The axial thermal error of the spindle is the output. Data obtained from tests 1 to 3 and tests 5 to 9 in Section 3 are used to develop the MR model and train BP network. Data collected at test 4 are employed to verify the prediction performance.

4.1 MR modeling

4.1.1 Data filtering for MR model

Generally, the abnormal data caused by noise, operational error, or other factors are mixed in the measured data. They are detrimental to the accuracy of modeling. For MR modeling, the confidence intervals on the residuals are taken as the criterion of data filtering. The results of the computation are shown in Fig. 12. Residuals larger than expected in 95 % are shown in red with triangular shape. These data are regarded as outliers and should be eliminated.

4.1.2 Results of MR modeling

After data filtering, MR model is established based on multiple variables. The function of the MR model is shown in Equation 13.

$$\begin{aligned} Y = {} & 36.2169 + (-3.7112)T_1^i + 5.2859T_2^i + 3.2123T_3^i + 3.8014T_4{}^i + 1.1819T_5^i + 2.8628T_6^i \\ & +(-7.0036)T_7^i + (-0.7733)T_8^i + (-1.4223)T_9^i + 0.8816T_{10}^i + 1.1399T_{11}^i + 3.1834T_{12}^i \\ & +2.0085T_{13}^i + (-0.016)T_{14}^i + 0.5982T_{15}^i + (-0.0002)v^i + 3.5514T_1^{i-1} + (-8.1634)T_2^{i-1} \\ & +(-1.2495)T_3^{i-1} + (-5.113)T_4^{i-1} + 0.335T_5^{i-1} + (-3.7186)T_6^{i-1} + 6.435T_7^{i-1} + 0.2906T_8^{i-1} \\ & +0.5038T_9^{i-1} + (-0.0105)T_{10}^{i-1} + (-0.0873)T_{11}^{i-1} + (-2.5182)T_{12}^{i-1} + (-0.1703)T_{13}^{i-1} \\ & +(-0.0305)T_{14}^{i-1} + (-2.7+)T_{15}^{i-1} + (-0.0002)v^{i-1} + (-5.1547)\Delta t + 0.9182Y^{i-1} \end{aligned} \tag{13}$$

where $T_1^i \sim T_{15}^i$ and $T_1^{i-1} \sim T_{15}^{i-1}$ are temperature data, Y and Y^{i-1} are the axial thermal errors of the spindle, v^i and v^{i-1} are the spindle speeds at moment t_i and t_{i-1}; $\triangle t$ is the time lag between t_i and t_{i-1}.

The fitting and the prediction results of MR model are shown in Fig. 13. The errors between the measured data and curve-fitting and prediction results are in the range of −2.5 to +2.5 μm and −6 to +10 μm, respectively. In order to verify the correctness and the effectiveness of modeling based on multiple variables which have been filtered, other two groups of input variables are used for MR modeling. Fitting and prediction results are shown in Table 3.

MSE is widely used to assess the quality of an estimator or a set of predictions in terms of its variation and degree of bias. Here, the less the MSE is, the better

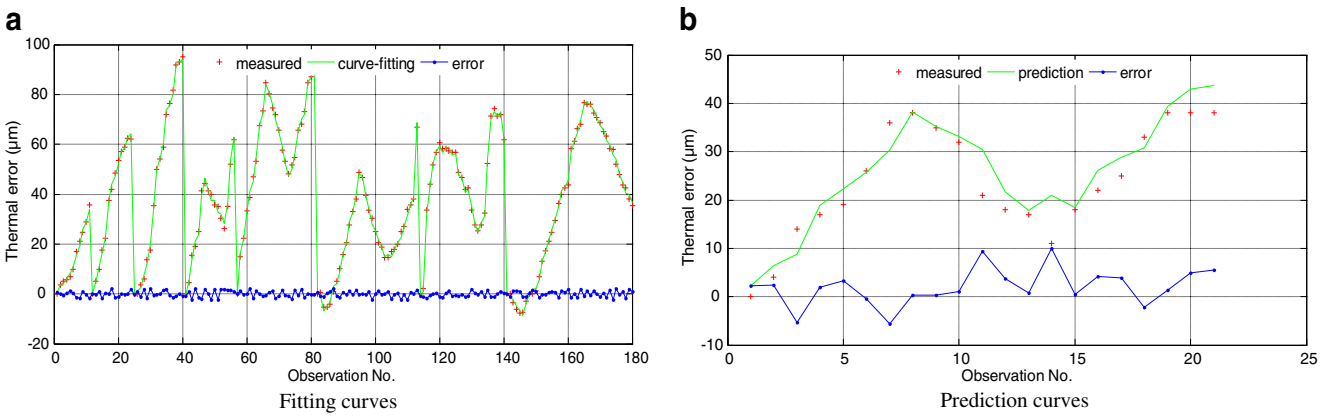

Fig. 13 Results of multiple regression modeling. **a** Fitting curves, **b** prediction curves

Table 3 Fitting and prediction results of MR modeling based on different data

Number	Data for modeling		Fitting results			Prediction results		
			Errors		MSE	Errors		MSE
	Data type	Data filtering	Min	Max		Min	Max	
1	Only temperatures	Not taken	−17.35	23.27	65.72	7.52	24.41	289.37
2	Temperature, spindle speed, historical data	Not taken	−8.61	6.51	5.60	−4.20	10.15	17.77
3		Have taken	−2.45	2.20	1.41	−5.61	10.02	18.31

MSE mean squared error

performances of the model are. According to Table 3, the fitting accuracy of the model established based on data 2 is better than the one built on data 1. The MSE of the former is about 8.5 % of the MSE of the latter. It means that it is necessary to take multiple variables as the input for modeling. The fitting accuracy of the model established based on data 3 is the highest. Its MSE is 1.41, which is only 2.1 and 25 % of the MSE of the models established based on data 1 and data 2, respectively. It illustrates that MR model accuracy can be further improved if the input data have been filtered. Besides, the prediction accuracy of the model established based on data 2 and data 3 is much better than the one built on data 1. MSE of models established based on data 2 and data 3 is about 6.1 and 6.3 % of MSE of the model established based on data 1, respectively. It illustrates that taking multiple variables as input data for modeling could improve the prediction performance. The prediction performance is not greatly improved after data filtering (MSE based on data 2/3= 17.77/18.31). This may be because that the robustness of MR model is limited.

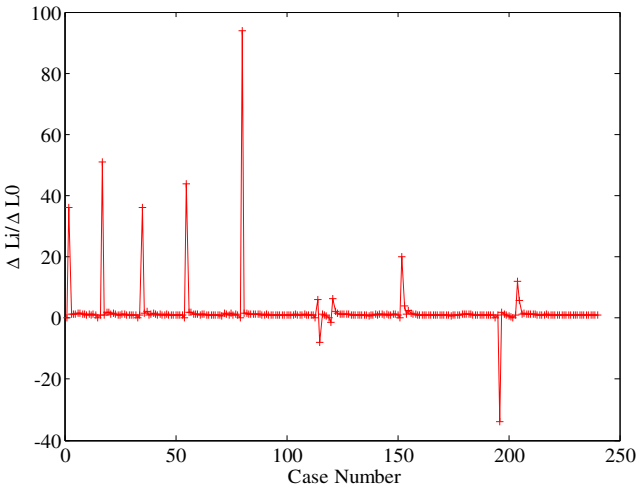

Fig. 14 Results of calculation based on the theory of thermal deformation

4.2 BP modeling

4.2.1 Data filtering for BP model

Here, the data for BP modeling are filtered based on the theory of thermal deformation (function 12). To make it easy to follow, the equation is showed again as following:

$$\Delta \mathrm{L} = \frac{\alpha L A (T_i - T_{i-1})}{\frac{L}{Ej} + \frac{A}{j^2}}$$

For simplicity, the original length (L), modulus of elasticity (E), the axial stiffness (j), and the area of the cross section (A) are considered as constant. Therefore, Equation 12 is changed to Equation 14:

$$\Delta \mathrm{L} = \alpha \cdot L \cdot C \cdot (T_i - T_{i-1}) \tag{14}$$

Here, C is the constant.

Considering that the thermal expansion coefficient of the materials used in the spindle system is very small [25], Equation 14 is converted to Equation 15 and then simplified into Equation 16.

$$\begin{cases} \dfrac{\Delta L_1}{L} = \alpha C (T_1 - T_0) = \alpha C \Delta T_1 \\ \dfrac{\Delta L_{i+1}}{\Delta L_i} = \dfrac{\Delta T_{i+1}}{\Delta T_i}(1 + \alpha C \Delta T_{i+1}) \quad \Delta T_i = T_i - T_0 \quad \Delta L_i = L_i - L \end{cases} \tag{15}$$

$$\frac{\Delta L_{i+1}}{\Delta L_i} = \frac{\Delta T_{i+1}}{\Delta T_i}; \quad \Delta T_i = T_i - T_0 \quad \Delta L_i = L_i - L \tag{16}$$

where T_0 is the initial temperature of the spindle.

According to the results of calculation based on Equations 15 and 16, almost 90 % of the data are in the range of

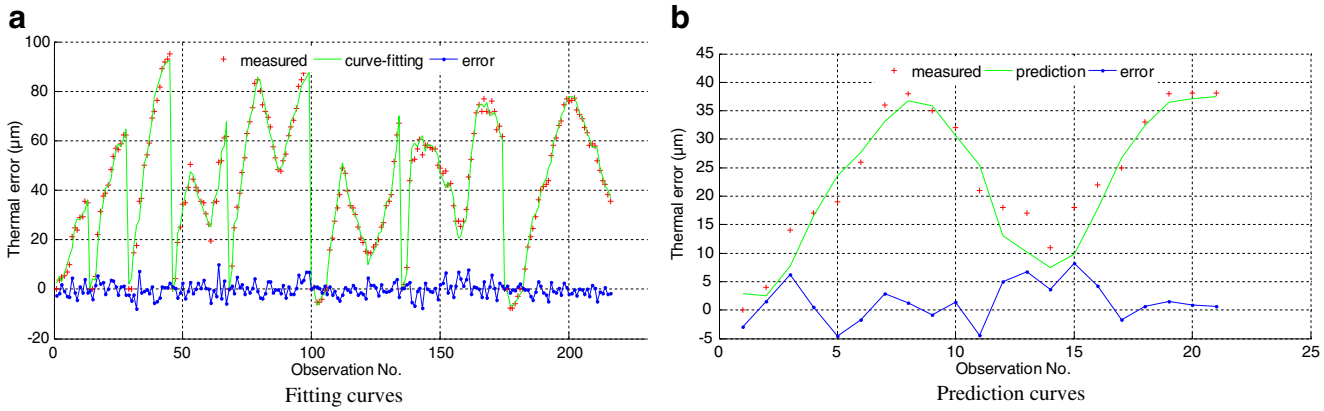

Fig. 15 Results of BP modeling. **a** Fitting curves, **b** prediction curves

−1.5 to 1.5 (Fig. 14). The data out of the range are regarded as the outliers and needed to be eliminated.

4.2.2 Results of BP modeling

The neural network is useful for mapping the relationship between multivariable inputs and outputs [26]. BP is one of the most popular methods of neural network [27] due to the satisfying accuracy and good robustness. Before training the BP network, the inputs and the targets are normalized by function "mapminmax" in MATLAB. After normalizing, the data become dimensionless and fall in the range [−1, 1], which helps to accelerate the training speed of BP network.

Figure 15 shows the results of BP modeling based on the filtered data including temperatures, the spindle speed, and the historical data. The errors between the test data and curve-fitting results are in the range of −10 to +10 μm which is acceptable although it is not as high as MR modeling. In addition, the prediction performance of BP modeling is great. Almost all of the errors between the data measured and predicted are limited in the range of −5 to +10 μm. Similarly, the results of BP modeling based on three different groups of input variables (Table 4) are used to verify the correctness and effectiveness of modeling based on multiple variables and to emphasize the meaning of the data filtering.

From Table 4, it can be seen that the fitting and prediction accuracy of BP model based on data 2 are better than the one built on data 1. The former MSE of fitting and prediction results are about 14.8 and 36.9 while the latter are 50.3 and 82.8, respectively. The model established based on data 3 has the highest fitting and prediction accuracy (MSE=8.2/13.5). Its fitting MSE is only 16.4 and 55.7 % of the MSE of models established based on data 1 and data 2, while the prediction MSE is about 16.3 and 36.5 %, respectively. It means that taking multiple variables as the inputs for modeling can definitely enhance the accuracy and robustness of the BP model. Furthermore, data filtering can further improve the model performance.

In conclusion, the results of MR and BP modeling verify the correctness and the necessity of modeling based on multiple variables and implementing data filtering. The models with good accuracy and robustness can be used for the further thermal error compensation.

4.3 Relative importance of variables

In multivariable studies, there is an ambition to compare the relative importance of different variables. One of the most commonly used methods is the standardized regression coefficients. The rank order of the standardized regression

Table 4 Fitting and prediction results of BP modeling based on different data

Number	Data for modeling		Fitting results			Prediction results		
			Errors		MSE	Errors		MSE
	Data type	Data filtering	Min	Max		Min	Max	
1	Only temperatures	Not taken	–20.8781	19.6508	50.3428	–15.7547	0.5880	82.8370
2	Temperature, spindle speed, historical data	Not taken	–12.9982	10.2513	14.7897	−13.3429	3.1407	36.8886
3		Have taken	−8.0014	9.9291	8.2433	−4.5721	8.1990	13.4773

MSE mean squared error

Table 5 Rank and absolute value of standardized regression coefficients

Rank	1	2	3	4	5	6	7	8	9	10	11	12
Predictor	T_{15}^{i}	T_{13}^{i}	T_{4}^{i-1}	T_{3}^{i-1}	T_{11}^{i}	T_{7}^{i-1}	T_{9}^{i}	T_{9}^{i-1}	T_{10}^{i-1}	T_{10}^{i}	T_{5}^{i-1}	T_{6}^{i-1}
Value	2.269	2.141	2.104	2.08	1.63	1.6	1.389	1.314	1.239	1.009	0.962	0.951
Rank	13	14	15	16	17	18	19	20	21	22	23	24
Predictor	T_{7}^{i}	T_{6}^{i}	T_{15}^{i-1}	T_{12}^{i-1}	T_{3}^{i}	T_{2}^{i}	T_{1}^{i-1}	T_{11}^{i-1}	T_{5}^{i}	T_{13}^{i-1}	T_{12}^{i}	v^{i}
Value	0.862	0.856	0.698	0.572	0.512	0.487	0.472	0.369	0.362	0.264	0.211	0.145
Rank	25	26	27	28	29	30	31	32	33	34		
Predictor	T_{11}^{i}	T_{8}^{i-1}	Y^{i-1}	T_{14}^{i-1}	T_{2}^{i-1}	T_{8}^{i}	v^{i-1}	$\triangle t$	T_{14}^{i}	T_{4}^{i}		
Value	0.117	0.092	0.055	0.032	0.026	0.02	0.013	0.013	0.011	0.002		

coefficients(absolute value) reveals the influences of the predictors on the dependent variable [28]. In this article, the temperatures, the spindle speed, and historical running conditions ($T_1^i \sim T_{15}^i$, v^i, $T_1^{i-1} \sim T_{15}^{i-1}$, v^{i-1}, $\triangle t$, and Y^{i-1}) are predictors, while the thermal error is the dependent variable. The standardized regression coefficients are computed and sorted by SPSS software (Table 5).

According to Table 5, the standardized regression coefficients of 15# and 13# are the top two. Possibly this is because that 15# and 13# temperature sensors are placed close to the rear bearing which is the heat source with the highest temperature. The temperatures of two sides and the top of the spindle box (4#, 3#, 7#) at previous t_{i-1} moment have severe impacts on the thermal error as they rank third, fourth, and sixth, respectively. The coefficient of present motor temperature (11#) is in fifth place. The oil temperatures at the present and previous times (T_9^i, T_9^{i-1}, T_{10}^i, T_{10}^{i-1}) rank seventh to tenth, respectively. Besides, the present spindle speed (v^i), the previous thermal error of the spindle (Y^{i-1}), and the time lag between t_i and t_{i-1} ($\triangle t$) rank 24th, 27th, and 32nd, respectively. The ranking demonstrates that the historical temperature plays a very important role in thermal error modeling as there are five temperatures at previous time (t_{i-1}) rank in the top 10 of the most significant predictors. In addition, the ranking can be used as a new criterion for optimal temperature variable selection [29] in the future because it can reflect the influences of the predictors on the dependent variable.

5 Conclusions

1. The thermal error is determined not only by temperatures but also by multiple variables such as the spindle speed, the historical spindle temperature, the historical thermal error, and the time lag between the present and previous times.
2. Multiple variables are taken as the input data for optimal spindle thermal error modeling in this paper. Two common multivariable modeling methods, MR and BP, are applied to establish models. The modeling results demonstrate that models built on multiple variables have better fitting and prediction accuracy than the ones based only on temperatures.
3. Data filtering can help to further improve the accuracy and the robustness of the thermal error model.
4. Standardized regression coefficients are computed to determine the relative importance of multiple variables to the thermal error. The ranking of the coefficients reveals that historical temperature plays a very important role in the thermal error modeling. Therefore, it can be used as a new criterion for optimal temperature variable selection in the future research.

Acknowledgments First of all, the author would like to express gratitude to Professor Zhao and Professor Lu for the valuable guidance on the research and experiments. Secondly, thank Professor Chen and Dr. Wu for their helpful recommendations on the paper structure organizing and English writing. Finally, it is gratefully acknowledged that the work has been supported by the State Key Laboratory for Manufacturing System Engineering and National Science and Technology Major Project of China (2012ZX04005011).

References

1. Gomez-Acedo E, Olarra A, Lopez de la Calle LN (2012) A method for thermal characterization and modeling of large gantry-type machine tools. Int J Adv Manuf Technol 62(9–12):875–886. doi:10.1007/s00170-011-3879-0
2. Junyong X, Youmin H, Bo W, Tielin S (2009) Research on thermal dynamics characteristics and modeling approach of ball screw. Int J Adv Manuf Technol 43(5–6):421–430. doi:10.1007/s00170-008-1723-y
3. Mou J (1997) A systematic approach to enhance machine tool accuracy for precision manufacturing. Int J Mach Tools Manuf 37(5):669–685
4. Bryan J (1990) International status of thermal error research (1990). CIRP Ann Manuf Technol 39(2):645–656
5. Lee J-H, Yang S-H (2002) Statistical optimization and assessment of a thermal error model for CNC machine tools. Int J Mach Tools Manuf 42(1):147–155
6. Wang Y-C, Kao M-c, Chang C-P (2011) Investigation on the spindle thermal displacement and its compensation of precision cutter grinders. Measurement 44(6):1183–1187
7. Weck M, McKeown P, Bonse R, Herbst U (1995) Reduction and compensation of thermal errors in machine tools. CIRP Ann Manuf Technol 44(2):589–598

8. Hsieh K-H, Chen T-R, Chang P, Tang C-H (2012) Thermal growth measurement and compensation for integrated spindles. Int J Adv Manuf Technol 64(5–8):889–901. doi:10.1007/s00170-012-4041-3
9. Ramesh R, Mannan M, Poo A (2000) Error compensation in machine tools—a review: Part II: thermal errors. Int J Mach Tools Manuf 40(9):1257–1284
10. Takada K, Tanabe I (1987) Basic study on thermal deformation of machine tool structure composed of epoxy resin concrete and cast iron. Bull Jpn Soc Precis Eng 21(3):173–178
11. Chen J-S (1996) Neural network-based modelling and error compensation of thermally-induced spindle errors. Int J Adv Manuf Technol 12(4):303–308. doi:10.1007/BF01239617
12. Tseng P-C (1997) A real-time thermal inaccuracy compensation method on a machining centre. Int J Adv Manuf Technol 13(3): 182–190. doi:10.1007/BF01305870
13. Yang J, Ren Y, Liu G, Zhao H, Dou X, Chen W, He S (2005) Testing, variable selecting and modeling of thermal errors on an INDEX-G200 turning center. Int J Adv Manuf Technol 26(7–8):814–818
14. Chen J, Yuan J, Ni J (1996) Thermal error modelling for real-time error compensation. Int J Adv Manuf Technol 12(4):266–275
15. Ramesh R, Mannan M, Poo A (2002) Support vector machines model for classification of thermal error in machine tools. Int J Adv Manuf Technol 20(2):114–120
16. Li Y, Yang J, Gelvis T, Li Y (2008) Optimization of measuring points for machine tool thermal error based on grey system theory. Int J Adv Manuf Technol 35(7–8):745–750
17. Li X (2001) Real-time prediction of workpiece errors for a CNC turning centre, Part 2. Modelling and estimation of thermally induced errors. Int J Adv Manuf Technol 17(9):654–658
18. Yang Z, Sun M, Li W, Liang W (2011) Modified Elman network for thermal deformation compensation modeling in machine tools. Int J Adv Manuf Technol 54(5–8):669–676
19. Ahn KG, Cho DW (1999) In-process modelling and estimation of thermally induced errors of a machine tool during cutting. Int J Adv Manuf Technol 15(4):299–304. doi:10.1007/s001700050070
20. Chen J-S, Hsu W-Y (2003) Characterizations and models for the thermal growth of a motorized high speed spindle. Int J Mach Tools Manuf 43(11):1163–1170
21. Haitao Z, Jianguo Y, Jinhua S (2007) Simulation of thermal behavior of a CNC machine tool spindle. Int J Mach Tools Manuf 47(6):1003–1010. doi:10.1016/j.ijmachtools.2006.06.018
22. Harris TA (1991) Rolling bearing analysis. Wiley, New York
23. Lienhard JH, Lienhard J (2000) A heat transfer textbook. Phlogiston Press, Cambridge, Massachusetts
24. Bossmanns B, Tu JF (1999) A thermal model for high speed motorized spindles. Int J Mach Tools Manuf 39(9):1345–1366
25. Li Y, Zhao W Axial thermal error compensation method for the spindle of a precision horizontal machining center. In: Mechatronics and Automation (ICMA), 2012 International Conference on, 2012. IEEE, pp 2319-2323
26. Ruijun L, Wenhua Y, Zhang HH, Qifan Y (2012) The thermal error optimization models for CNC machine tools. Int J Adv Manuf Technol 63(9–12):1167–1176
27. Mize CD, Ziegert JC (2000) Neural network thermal error compensation of a machining center. Precis Eng 24(4):338–346
28. Menard S (2004) Six approaches to calculating standardized logistic regression coefficients. The American Statistician 58 (3)
29. Lo C-H, Yuan J, Ni J (1999) Optimal temperature variable selection by grouping approach for thermal error modeling and compensation. Int J Mach Tools Manuf 39(9):1383–1396